First-Principles-Based Surface Phase Diagram of Fully Relaxed Binary Alloy Surfaces

O. Wieckhorst, S. Müller, L. Hammer, and K. Heinz

University Erlangen-Nürnberg, Lehrstuhl für Festkörperphysik, Staudtstrasse 7, D-91058 Erlangen, Germany

(Received 23 December 2003; published 14 May 2004)

The combination of density-functional theory (DFT) calculations of geometrically fully relaxed binary alloy surfaces with concepts from statistical physics is applied to construct a DFT-based phase diagram for a binary alloy surface. As a first example, we studied the appearance of Co antisite atoms at CoAl(100) surfaces. The structural parameters as multilayer relaxations, surface buckling, lateral order, and segregation profile of the predicted stable surface phases are in excellent agreement with experimental structure determinations applying low-energy electron diffraction.

DOI: 10.1103/PhysRevLett.92.195503 PACS numbers: 68.35.Dv, 61.14.Hg, 61.82.Bg, 71.15.Mb

Today, powerful computer programs based on density-functional theory (DFT) allow the reliable prediction of important bulk properties of alloys. However, the situation is less favorable when the surface comes into play, in particular, as there the stoichiometry can strongly deviate from that in the bulk. This is due to surface segregation taking place in almost all disordered metal alloys by control through the chemical equilibrium between near-surface layers and the bulk. In *ordering* alloys (intermetallic compounds), however, the segregation of one component to the surface should be unfavorable as it involves, e.g., in case of *AB* alloys, the occupation of adjacent sites by identical atoms, i.e., the formation of *antisites*. Nevertheless, antisites have been detected, e.g., in the (100) surface of the *B*2 (or CsCl-type) phase of CoAl [1], which should be purely Al-terminated (as this is clearly favored over Co termination [2]). The existence of Co atoms in the top layer (*Co antisites*) can be explained by the fact that — though the sample owns a concentration of nominally 50% Al—there can be tiny deviations from this ideal stoichiometry in the real crystal [1]. They come by Co antisites rather than energetically less favorable Al vacancies [3]. The latter's creation costs 1.59 eV [3] and our DFT calculations yield a segregation energy of -1.81 eV. As a consequence, the energy balance for the segregation of two vacancies (equivalent to antisite formation at the surface) is $-0.22 \times 2 = -0.44$ eV, i.e., much less favorable than the value of -0.85 eV [1] for the segregation of antisites existing in the bulk. Therefore, we can neglect vacancy segregation.

In this Letter we offer a rather general description of surface segregation including the antisite ordering within the surface. We concentrate on the above example and construct the phase diagram of the surface without any input of empirical parameters, revealing the dependence of ordering on temperature and on the bulk concentration of antisites. We show that the predictions are in excellent agreement with the crystallographic-chemical properties of the surface as resulting from quantitative low-energy electron diffraction (LEED) or the appearance of diffuse LEED spots indicative for short-range ordering.

Our strategy is as follows: (i) First, we calculate the energy $E_{\mathrm{AS}}(x)$ necessary to create a certain concentration of Co antisites in the CoAl bulk described by the Co bulk concentration, $x > 0.5$. For this we apply DFT combined with the cluster-expansion (CE) technique [4], which allows the treatment of large unit cells necessary to access small antisite concentrations. (ii) Second, we derive an equation for the surface formation enthalpy Σ which depends on both the antisites' ordering and concentration in the surface. Their energetics is described by DFT calculations for a surface slab and the chemical potentials of the different species involved. Here, equilibrium with the bulk must be considered, by which the quantity E_{AS} calculated in step (i) gets involved. Eventually, the chemical potential of the antisites within the surface slab is transformed to the temperature scale yielding the surface phase diagram in the (T, x) plane.

The Co antisite formation energy in the bulk to be calculated in step (i) can be expressed by

$$E_{\mathrm{AS}}(x) = \frac{1}{N} \frac{E^b(x) - E^b(B2)}{x - 0.5}, \tag{1}$$

where $E^b(x)$ is the bulk energy for a crystal with a total of N atoms and a Co antisite concentration $x_{\mathrm{AS}} = x - 0.5$, while $E^b(B2) = E^b(x = 0.5)$ corresponds to the ideal $B2$-ordered bulk. $E^b(B2)$ can be calculated by DFT and, in principle, this is true for $E^b(x)$ as well. Yet, the latter's calculation for, e.g., a 0.1% antisite concentration requires already a unit cell of 500 $B2$ cubes. This corresponds to a rather demanding DFT calculation which, in order to account for a possible concentration dependence of E_{AS}, has to be repeated for many values of x. Additionally, a DFT calculation for a *random* distribution of antisites — which is reasonable to assume — practically would be impossible. Therefore, we apply the CE method [4] where the energy wanted results as

$$E^b(x) = N \sum_F^{N_F} D_F \bar{\Pi}_F(\sigma_x) J_F \tag{2}$$

with the structure built up by N_F atomic figures as dimers,

trimers, quadrumers, and so on. D_F gives the number of such figures of symmetry class F and J_F is the corresponding characteristic energy, which has to be determined separately as input to the CE. The quantities $\bar{\Pi}_F(\sigma_x)$ depend on the distribution of the antisites, i.e., their configuration σ at the concentration x which, for the present case is random, $\sigma_x = \sigma_x^{\text{ran}}$. Clearly, we need the energies J_F as the crucial input to Eq. (2). They come by DFT calculations for a set of $M > N_F$ structures with Co concentration x_i within a comparably small unit cell [5] (comprising, in the present case, 4 $B2$ unit cells in each direction equivalent to a total of 128 atoms). The corresponding energies, $E^b_{\text{DFT}}(x_i)$, were calculated using plane waves and ultrasoft pseudopotentials [6] (VASP code [7]), where full relaxation of the structure was allowed in each case. Then these small sized structures are again represented by a cluster expansion, where an Ising-like representation is used to calculate $\bar{\Pi}_F(\sigma_{x_i})$ [2,4]. Eventually, the quantities J_F result by the minimization of a weighted mean-square deviation between the DFT calculated energies and the CE representation [5]. So, $E^b(x)$ can be calculated by Eq. (2) for any antisite concentration $x_{\text{AS}} = x - 0.5$ applying $\sigma_x = \sigma_x^{\text{ran}}$. Then, $E_{\text{AS}}(x)$ results via Eq. (1), where the energy zero refers to that of the elemental crystals of Co and Al (with bcc structure assumed). Using the latters' chemical potentials, $\mu^{\text{elem}}_{\text{Co,AL}}$, the quantity $E^*_{\text{AS}}(x) = E_{\text{AS}}(x) - (\mu^{\text{elem}}_{\text{Al}} - \mu^{\text{elem}}_{\text{Co}})$ refers to the energy of the $B2$-ordered CoAl bulk, and this quantity is displayed in the inset of Fig. 1. As is obvious, the antisites interact so that E_{AS} becomes somewhat concentration dependent for not too low concentrations.

In the next step (ii), we describe the energetics of the surface. We need to switch to a thermodynamic description because we want to find the antisite surface concentration in equilibrium with the bulk. As we expect no Al antisites on the Co sublattice because of their comparably large formation energy [3], we have to deal with only three different kinds of particles within the surface unit cell, namely, N_{AS} Co antisites, N_{Al} Al atoms on the Al sublattice, and N_{Co} Co atoms on the Co sublattice. In equilibrium, their surface chemical potentials μ_{AS}, μ_{Al}, and μ_{Co} in the surface slab must be related to the corresponding values in the bulk. We choose these chemical potentials as variables so that the surface's Gibbs function (surface formation energy per atom)

$$\Sigma = \frac{1}{A_s}(G_S - N_{\text{AS}}\mu_{\text{AS}} - N_{\text{Al}}\mu_{\text{Al}} - N_{\text{Co}}\mu_{\text{Co}}) \quad (3)$$

in a stable phase assumes a minimum as a function of the potentials μ_i and temperature T. Here, A_s is the number of surface atoms per unit cell and G_S the free energy, $G_S(T, N_{\text{AS}}, N_{\text{Al}}, N_{\text{Co}}) = E_{\text{DFT}}(N_{\text{AS}}, N_{\text{Al}}, N_{\text{Co}}) - TS$. In the latter we can neglect the entropic contribution as its vibrational part (< 10 meV/atom at 1000 K [8]) is small compared to the antisite energy and is of even less influence when different structures are compared so that only entropy differences are involved. Also, as these structures are expected to be at least short-range ordered, the configurational part should be rather small, too. The neglect of the entropy term may somewhat influence the calculated phase boundaries, but the main features of the phase diagram should be preserved. Earlier investigations [9] successfully used the mean-field approach by applying a tight-binding Ising model with size-effect contributions.

Because of Al-antisites missing, the Co sublattice acts only as a constant "background" and μ_{Co} can be replaced by its bulk value. For both Co and Al, the bulk values derive from those of the elemental (bcc) crystals by $\mu^{\text{bulk}}_{\text{Co}} + \mu^{\text{bulk}}_{\text{Al}} = \mu^{\text{elem}}_{\text{Co}} + \mu^{\text{elem}}_{\text{Al}} + 2\Delta H_f$ where ΔH_f is the alloy formation enthalpy. So, we are left with only two types of particles, namely, Al atoms and Co antisites on the Al sublattice. The antisites in the surface come by a reaction in which a concentration of $(2x - 1)$ antisites are created in the slab so that only a concentration of $(2 - 2x)$ Al atoms remains (note that concentrations are doubled when referring only to the Al sublattice). The reaction comes by the surface's coupling to the bulk crystal which acts as an antisite reservoir, so that the equation

$$(2x - 1)\mu_{\text{AS}} + (2 - 2x)\mu_{\text{Al}} = \mu^{\text{bulk}}_{\text{Al}} + (2x - 1)E_{\text{AS}} \quad (4)$$

must be met, in which both sides are equal to $\mu^{\text{bulk}}(\text{Co}_{2x-1}\text{Al}_{2-2x})$. By the use of Eq. (4) one of the two surface chemical potentials can be eliminated with the variation of the other being sufficient to construct the phase diagram aimed for. Yet, this variation is restricted to maximum and minimum values. So, $\mu_{\text{Al}} \le \mu^{\text{bulk}}_{\text{Al}} - E_{\text{AS}}(x)$ must be met because for larger μ_{Al} no antisites at all would be possible in the surface slab. With Eq. (4) this transforms to a lower limit $\mu^{\text{min}}_{\text{AS}} = \mu^{\text{bulk}}_{\text{Al}} + E_{\text{AS}}(x)/(2x - 1) \le \mu_{\text{AS}}$. On the other hand, $\mu^{\text{max}}_{\text{AS}} = \mu^{\text{bulk}}_{\text{Al}} + E_{\text{AS}}(x) \ge \mu_{\text{AS}}$ must hold since otherwise the whole Al sublattice would consist of Co antisites. As $\mu^{\text{min}}_{\text{AS}}$ and $\mu^{\text{max}}_{\text{AS}}$ own the same energy offset ($\mu^{\text{bulk}}_{\text{Al}}$), it is reasonable to consider only $\Delta\mu_{\text{AS}} = \mu_{\text{AS}} - \mu^{\text{max}}_{\text{AS}}$, which, with $\eta(x) = (2 - 2x)/(2x - 1)$ varies in the range

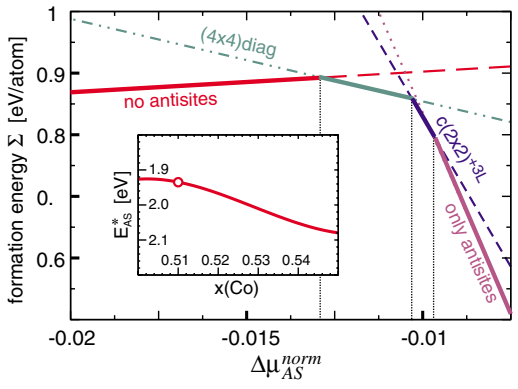

FIG. 1 (color online). Stability diagram for $x_{\text{Co}} = 0.51$. In the inset the dependence of the antisite energy E^*_{AS} as a function of the Co bulk concentration x(Co) is shown with the value marked at which the stability diagram was calculated.

$$\eta(x)E_{\mathrm{AS}}(x) \leq \Delta\mu_{\mathrm{AS}} \leq 0 \quad (5)$$

or after normalization, $\Delta\mu_{\mathrm{AS}}^{\mathrm{norm}} = \Delta\mu_{\mathrm{AS}}/|\eta(x)E_{\mathrm{AS}}(x)|$, in the equivalent, dimensionless range

$$-1 \leq \Delta\mu_{\mathrm{AS}}^{\mathrm{norm}} \leq 0. \quad (6)$$

Inserting the above equations into Eq. (3) leads to

$$\Sigma = \frac{1}{A_S}\Big[E_{\mathrm{DFT}} - N_{\mathrm{AS}}[\mu_{\mathrm{Al}}^{\mathrm{bulk}} + E_{\mathrm{AS}}(x)] - N_{\mathrm{Al}}\mu_{\mathrm{Al}}^{\mathrm{bulk}} - N_{\mathrm{Co}}\mu_{\mathrm{Co}}^{\mathrm{bulk}} - \left(N_{\mathrm{AS}} - \frac{N_{\mathrm{Al}}}{\eta(x)}\right)|\eta(x)E_{\mathrm{AS}}(x)|\Delta\mu_{\mathrm{AS}}^{\mathrm{norm}}\Big]. \quad (7)$$

The energies E_{DFT} were calculated, applying again the VASP code. As usual for surface calculations, an array of symmetric atomic slabs consisting of (here 9) alternating Al and Co layers and separated by vacuum (here equivalent to 11 layers) was considered. Co antisites were allowed only in the top and third layers of the nominally Al-terminated slab (note the even-numbered layers belong to the Co sublattice of $B2$-CoAl). Fortunately, in recent work the stability of phases with antisites only in the top layer has already been investigated [2]. *All* superstructures with unitcells made up by up to 20 basis atoms in the top layer were considered with only a few of them found to be stable. Restricting to those in the present work we additionally allowed for superstructures also in the third layer, resulting in a total of 60 trial structures. Of course, also structures with no antisites at all as well as complete antisite occupation of the Al sublattice (phase separation) were considered. In all phases atomic movements were allowed in order to account for energy-lowering geometric relaxations.

Only the last term of Eq. (7) contains $\Delta\mu_{\mathrm{AS}}^{\mathrm{norm}}$, which controls the surface stoichiometry, while the remaining parts are constant for a given bulk antisite concentration. In practice, for a fixed x the corresponding antisite energy $E_{\mathrm{AS}}(x)$ is determined via Eq. (1) and then $\Sigma = \Sigma(x)$ can be calculated from Eq. (7) for a certain trial surface termination model. By variation of $\Delta\mu_{\mathrm{AS}}^{\mathrm{norm}}$ the stability of the different trial surface terminations and the stability ranges of the stable phases can be determined. Part of such a stability diagram for a selected bulk stoichiometry, $x = 0.51$, is shown in Fig. 1 where only the lines of the stable four surface structures are shown. The figure shows that both the pure (i.e., antisite-free) Al termination and phase separation, with the first and third layers consisting *only* of antisite atoms, are stable phases. Besides, only two stable superstructures—in which the Al atoms together with Co antisites in the top layer exhibit chemical order—are found. They are displayed in Fig. 2. In the (4×4)diag superstructure [Wood notation: $(2\sqrt{2} \times \sqrt{2})R45°$] diagonal rows of antisites reside in the top layer with fourfold vertical and horizontal spacings in between, and below the top layer there is unperturbed $B2$ order. The other stable superstructure, $c(2 \times 2)^{+3\mathrm{L}}$, owns 50% antisites in the top layer and, additionally, the third layer fully consists of antisites.

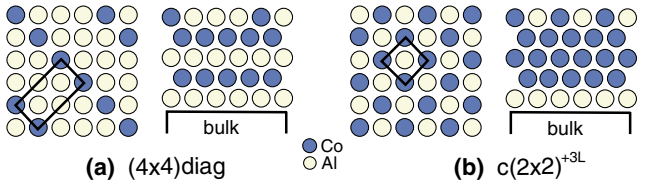

FIG. 2 (color online). Ball models of the (a) (4×4)diag and (b) $c(2 \times 2)^{+3\mathrm{L}}$ phase in top (left) and side (right) views in each case. The lateral surface unit cells are indicated in the top views.

In order to construct the surface phase diagram, the just described stability determination of the different phases was repeated as a function of x (no other stable phases appeared than those already mentioned). Additionally, the chemical potential scale had to be transferred to the temperature scale. For this purpose the interaction between antisites was neglected, so that they can be treated as independent particles. The Bragg-Williams approach yields $\Delta\mu_{\mathrm{AS}} = k_B T \ln(2x - 1)$, and eventually the phase diagram of the surface results as shown in Fig. 3. Again, there are two limiting cases, namely, that of phase separation at low temperatures and that of ideal termination at high temperatures. In between them there is a large stability region for the (4×4)diag phase and a rather small one for the $c(2 \times 2)^{+3\mathrm{L}}$ phase in which the surface exhibits chemical order. Obviously, at high T there are no antisites at the surface because entropy favors a random distribution. With T lowered, antisites concentrate first in the top layer because there, due to the lower coordination, the energetic situation is more favorable than in the bulk. Yet, this does not lead to a complete Co top layer because of the high surface energy involved [1]. Instead, with T further lowered the $c(2 \times 2)^{+3\mathrm{L}}$ phase develops with antisites also in the third layer. Eventually, at even lower T there is complete phase separation.

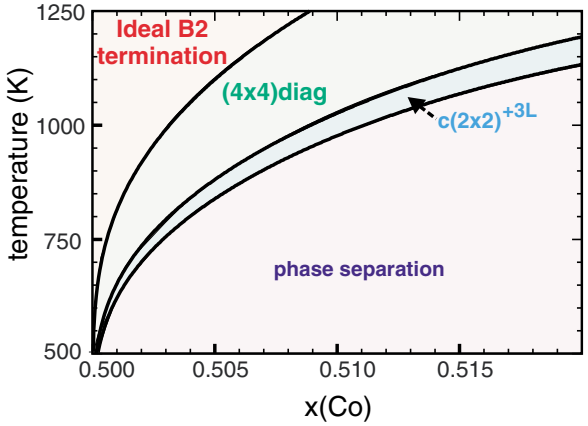

FIG. 3 (color online). Calculated surface phase diagram for CoAl(100).

For the validity of our approach it is important whether or not the two phases characterized by antisite ordering in a chemically mixed surface layer are paralleled by experiment. As mentioned, diffuse spots centered in the (1×1) bulk unit meshes are observed in LEED, indicative for a surface superstructure which, however, exhibits only short-range order. Both the (4×4)diag and the $c(2 \times 2)^{+3L}$ phase with their extra spots broadened may be the underlying local structures. As the intensities of diffuse spots cannot be measured reliably, only the integer-order spot intensities of such phases can be made to undergo a full dynamical LEED analysis. The perturbation method tensor LEED [10] implemented in the computer code used [11] was applied allowing for a simultaneous determination of the layer-dependent stoichiometry *and* the element specific positions of atoms in the surface [this is in spite of the average structure being of (1×1) symmetry] [12]. The structural parameters which, by input to model intensity calculations, reproduce the experimental intensities best (as judged by the Pendry R factor [13]) correspond to the experimentally determined parameter values. By comparison with their theoretical counterparts calculated by first principles as described above, the reliability of the present theoretical approach can be judged.

This procedure was applied to a CoAl crystal with, however, the exact off-stoichiometry unknown. To get a clean surface, sputtering and annealing was applied as usual. With Al preferentially sputtered, a Co rich surface slab results. Subsequent annealing restores, dependent on the annealing temperature, a certain stoichiometry in a subsurface region which, rather than the bulk, acts as an antisite reservoir for the very surface [14]. Two different annealing temperatures were applied and the sample then quenched to liquid air temperature for the LEED measurement, so that two different (unknown) subsurface antisite concentrations were frozen in, denoted "low" and "high" concentrations in the following. The parameters resulting from the LEED analyses are compared to those retrieved from DFT in Table I (the result for the low concentration phase was already used in Ref. [1]). It turns out that the low and high concentration phases can be clearly identified with the (4×4)diag and the $c(2 \times 2)^{+3L}$ superstructures, respectively. Given the accuracy of the LEED analyses and of the theoretical approach (with the various approximations used) the theory-experiment comparison is excellent in each case. The structural parameters differ by a few pm at most. The stoichiometric differences are modest, too, and might be due to some kinetics inhibiting full equilibration in the experiment at the temperature chosen. A seemingly characteristic feature of the surface, namely, the sign and amplitude of the top layer's buckling in the two phases, is also well reproduced. While in the (4×4)diag phase Co protrudes from the surface, this holds for Al in the $c(2 \times 2)^{+3L}$ structure. Obviously, the third layer antisite concentration controls the buckling in the top layer. More generally, it appears that the kind of substitutional order of antisite atoms in the surface has a considerable influence on the local geometry, where lacking long-range order (as present in the experiment) is of only slight influence, if any.

TABLE I. Comparison of structural parameters retrieved by quantitative LEED and DFT. The quantities $x_{\mathrm{AS}}^{1,3}$ denote the Co antisite concentrations in the top and third layers, b the atomic buckling in the top layer (i.e., the difference between outward displacements of Co and Al), and $d_{i,j}$ the spacing between layers i and j (d_b = bulk value).

	LEED[a] (low conc.)	DFT (4×4)diag	LEED (high conc.)	DFT $c(2 \times 2)^{+3L}$
x_{AS}^{1} [%]	30	25	55	50
x_{AS}^{3} [%]	15	0	80	100
b [Å]	+0.08	+0.08	−0.14	−0.19
d_{12} [Å]	1.38	1.38	1.31	1.31
d_{23} [Å]	1.46	1.46	1.47	1.43
d_{34} [Å]	1.42	1.43	1.43	1.40
d_{45} [Å]	1.43	1.43	1.44	1.44
d_b [Å]	1.43	1.43	1.43	1.43

[a]From Ref. [1].

In conclusion, we have shown that DFT calculations extended by a cluster expansion to large systems and combined with thermodynamics can be used to construct the stoichiometric-structural phase diagram of an alloy surface. The phases found are chemically and geometrically close to those determined experimentally. Their development depends strongly on temperature and bulk antisite concentration even though the latter might be very small.

[1] V. Blum *et al.*, Phys. Rev. Lett. **89**, 266102 (2002).
[2] S. Müller, J. Phys. Condens. Matter **15**, R1429 (2003).
[3] G. Bester *et al.*, Phys. Rev. B **60**, 14 492 (1999).
[4] J. M. Sanchez *et al.*, Physica (Amsterdam) **128A**, 334 (1984).
[5] G. D. Garbulsky and G. Ceder, Phys. Rev. B **51**, 67 (1995).
[6] G. Kresse and J. Hafner, J. Phys. Condens. Matter **6**, 8245 (1994).
[7] G. Kresse and J. Furthmüller, Comput. Mater. Sci. **6**, 15 (1996).
[8] K. Reuter and M. Scheffler, Phys. Rev. B **65**, 035406 (2002).
[9] G. Treglia *et al.*, Comput. Mater. Sci. **15**, 196 (1999).
[10] P. J. Rous *et al.*, Phys. Rev. Lett. **57**, 2951 (1986).
[11] V. Blum and K. Heinz, Comput. Phys. Commun. **134**, 392 (2001).
[12] K. Heinz, Rep. Prog. Phys. **58**, 637 (1995).
[13] J. B. Pendry, J. Phys. C **13**, 937 (1980).
[14] L. Hammer *et al.*, J. Phys. Condens. Matter **14**, 4145 (2002).